Kidney Diseases

Research Article

Kidney Dis 2025;11:302–318
DOI: 10.1159/000545663

Received: November 26, 2024
Accepted: March 12, 2025
Published online: April 6, 2025

Deciphering Intercellular Communication of the Immune Landscape within Autosomal Dominant Polycystic Kidney Disease Microenvironment at Single-Cell Resolution

Fei Liu[a] Xiaoyi Li[a] Qiuyu Li[a] Jinglan Gu[a] Qi Shi[b] Jiayi Song[b] Na Jiao[c] Jianhua Mao[a]

[a]Department of Nephrology, Children's Hospital, Zhejiang University School of Medicine, National Clinical Research Center for Child Health, Hangzhou, PR China; [b]School of Basic Medical Sciences & Forensic Medicine, Hangzhou Medical College, Hangzhou, PR China; [c]Department of Microbiology and Microbial Engineering, School of Life Sciences, Fudan University, Shanghai, PR China

Keywords

Autosomal dominant polycystic kidney disease · Single-cell transcriptome · Immune microenvironment · Macrophages · T cells · Fibroblasts

Abstract

Introduction: Autosomal dominant polycystic kidney disease (ADPKD) is a genetic disorder that often leads to end-stage renal disease, with disease progression deeply influenced by the renal microenvironment. This study aims to unravel the critical cellular types and their intricate interactions within the ADPKD microenvironment. ***Methods:*** Leveraging single-cell transcriptome data from seven ADPKD and three healthy human kidney samples, we systematically dissected the cellular landscape of the ADPKD microenvironment. Our approach included CellChat for cell-cell communication analysis, VISION for pathway enrichment analysis, pySCENIC for regulon activity calculation, and Monocle V3 for pseudotime trajectory construction. ***Results:*** We identified nine major cell lineages, with a notable increase of mononuclear phagocytes (MNPs), T cells, and fibroblasts in the ADPKD microenvironment. These cells collectively orchestrated a distinctive microenvironment, marked by complex intercellular networks. Notably, a specific subset of macrophages exhibited an "M2-like" phenotype, which was driven by IL-10 signaling from M1-like macrophages and contributed to cyst cell proliferation. Immunosuppression was predominantly mediated by CD4+ T cells, activated by macrophages through immune checkpoint pathways, such as PDL1 signaling. The fibrotic expansion was a cumulative effect of fibroblast activation and proliferation, modulated by macrophages and cyst-lining epithelial cells. ***Conclusion:*** This comprehensive investigation provides valuable insights into the diverse landscapes of the ADPKD microenvironment at single-cell resolution, emphasizing MNPs, T cells, and fibroblasts. The study unveils complex interactions among these cell types, shedding light on an understanding of the immunological aspect of ADPKD and proposing potential therapeutic targets.

Fei Liu and Xiaoyi Li contributed equally to this work.

karger@karger.com
www.karger.com/kdd

Correspondence to:
Na Jiao, najiao@fudan.edu.cn
Jianhua Mao, maojh88@zju.edu.cn

Introduction

Autosomal dominant polycystic kidney disease (ADPKD) is a monogenetic progressive kidney disease characterized by the bilateral development and enlargement of renal cysts, ultimately leading to increased kidney volume [1]. It ranks as the fourth leading cause of end-stage renal disease globally in adults [2]. ADPKD primarily arises from mutations in the PKD1 and PKD2 genes, responsible for encoding polycystin-1 and polycystin-2. The two proteins together form a heteromeric complex in the primary cilium of renal cells, functioning as a mechanically sensitive flow sensor in renal tubular epithelia [3].

While the genetic factors underlying ADPKD are well established, its progression is not solely attributed to genetics but also to the renal microenvironment, which comprises various cellular and extracellular matrix (ECM) components, such as immune cells and fibroblasts [4]. In renal studies, the concept of the microenvironment mainly emphasizes the complex interactions between different cell types, such as macrophages and fibroblasts, mediated by various signaling factors [5, 6]. Typically, the tumor microenvironment (TME) is crucial in shaping multiple pathogenetic features, including sustained tumor proliferation, evasion of immune destruction, and inflammation that promotes tumors. Interestingly, these aspects bear significant commonalities with ADPKD [7]. In renal cell cancer, targeting the TME to contain or eliminate cancer cells has emerged as a promising therapeutic approach, with multiple studies exploring ways to either stimulate or combat the TME components [8]. Hence, the microenvironment in ADPKD is increasingly considered an appealing therapy target, with immune cells within it presuming to play significant and multifaceted roles in disease progression, paralleling those observed in cancer. For example, macrophages have been demonstrated to contribute to cyst cell proliferation and cyst expansion through arginase-1, while the depletion of macrophages could restrain pathological enlargement of kidneys [9, 10]. Conversely, CD8+ T cells appeared to have a renoprotective role in ADPKD, promoting cyst apoptosis and reducing cyst proliferation [11]. Furthermore, transcriptome analyses have unveiled an enrichment of immune response and defense pathways in ADPKD [12].

Although initial insights were gleaned from bulk tissue analyses, which have limitations in unraveling cellular dynamics and heterogeneity, the emergence of single-cell sequencing (scRNA-seq) has revolutionized transcriptome characterization at the cellular level. This advancement enables the detailed identification of distinct cell types and their interactions, offering fresh perspectives in examining the microenvironment of kidney diseases [13–15]. Specifically, Muto et al. [16] utilized single-nuclei RNA sequencing (snRNA-seq) and single-nucleus assay for transposase accessible chromatin sequencing (snATAC-seq) to identify proximal tubular cells with a profibrotic failed-repair transcriptomic signature, along with pro-inflammatory collecting duct cells and fibroblasts in late stage ADPKD samples. Li et al. [17] employed scRNA-seq to dissect epithelial heterogeneity and cyst cell origin in human ADPKD and normal samples. In the Pkd1 mouse model, Li et al. [18] further explored the landscape of collecting duct cells and their intercellular communication with other cells, highlighting interactions such as migration inhibitory factor signaling with T/nature killer (NK) cells, fibroblasts, and macrophages, which were proposed to contribute to cyst proliferation. However, these works primarily focused on parenchyma cells and did not systematically characterize the immune microenvironment or fully describe the involved intercellular networks.

In our study, we conducted a comprehensive scRNA-seq analysis based on seven ADPKD samples and three healthy kidney samples, yielding a detailed cell atlas and intercellular interaction networks within the ADPKD microenvironment. Our findings underscored increased abundances of mononuclear phagocytes (MNPs), T cells, and fibroblasts in the ADPKD microenvironment, which collectively facilitate ADPKD advancement by creating an immunosuppressive environment, promoting cyst-lining epithelial proliferation, and driving fibrosis. In total, our study provides a systematical exploration of the MNPs, T cells, and fibroblasts in ADPKD and their intercellular networks, shedding new light on specific cell subpopulations as potential therapeutic targets.

Methods

Data Source

The raw scRNA-seq data, comprising seven human ADPKD samples and three normal kidney samples, were obtained from the publicly accessible NCBI Sequence Read Archive (SRA) using the BioProject accession numbers PRJNA679848 [17] and PRJNA544431 [19], respectively. Furthermore, transcriptomic data from bulk tissues originated from the Gene Expression Omnibus database (GEO), accessed under the identifier GSE7869 [20]. This dataset featured a comprehensive set of human

microarray profiles, including five minimally cystic tissue samples, five small cyst samples, five medium cyst samples, three large cyst samples, and three normal renal cortical samples. The corresponding relationships between sample ID and GEO identifier are listed in online supplementary Table S1 (for all online suppl. material, see https://doi.org/10.1159/000545663).

Data Preprocessing

We initiated our analysis by performing quality control on the scRNA-seq data using Seurat (version 4.3.0.1) [21]. We retained high-quality cells in the dataset by applying the following criteria: (1) cells with unique feature counts >500; (2) cells with total UMI counts between 500 and 25,000, and (3) cells with mitochondrial gene expression <20% and hemoglobin gene expression <5%. Additionally, genes expressed in fewer than 3 cells were also removed to enhance data integrity. From the remaining pool of the 93,483 cells, the gene expression dataset was subjected to normalization and scaling procedures. Subsequently, the dimension reduction based on the top 20 principal components was executed. Batch effect correction was further implemented with harmony (version 0.1.1) [22] to mitigate potential technical variations arising from distinct sources. We employed Local Inverse Simpson's Index (LISI), a metric assessing diversity within the neighborhood of a cell, to calculate the top two principal components to quantify batch correction effectiveness. A higher LISI indicated neighborhoods including cells from multiple batches, denoting a lower batch effect. The statistical significance between LISIs from pre-batch corrected and post-batch corrected datasets was assessed using a *t* test.

Major Cell Lineage Identification and Subclustering Analysis

Louvain clustering was employed on the nearest-neighbor graph using a resolution parameter of 0.7, resulting in 27 distinct clusters (online suppl. Fig. S1). These clusters were subsequently categorized into nine major cell types and were annotated through markers based on a combination of previous research [16, 23–26] and the CellMarker database [27]. To delineate cell subtypes within prominent lineages, the expression matrix of MNPs, T cells, and fibroblasts underwent a second-round normalization, scaling, and dimension reduction. The derived expression matrices were then utilized to construct distinct nearest-neighbor graphs. Subsequent Louvain subclustering was performed, employing resolution parameters of 0.3, 0.1, and 0.1 applied for MNPs, T cells, and fibroblasts, respectively. Notably, in the refined second-round clustering of T cells, it was observed that cluster 5 was marked by NK cell marker NCAM1 rather than T-cell markers, and cluster 7 lacked T-cell markers (online suppl. Fig. S2A). Consequently, these two clusters were excluded to refine the focus for downstream analyses. The classification of cell subtypes was mainly predicated on markers obtained from the CellMarker database [27]. Specifically, for MNP subtype identification, M1 and M2 scores derived from the differential expression genes (DEGs) outlined by Martinez et al. [28] were employed. Exhaustion and cytotoxicity scores for T cells [29] and ECM and collagen scores for fibroblast subtypes were also utilized [30] (online suppl. Table S2). These scores, represented by the mean expression of gene sets respectively, were employed to enhance the precision of subtype categorization.

Cell-Cell Communication Analysis

CellChat (version 1.6.1) [31] uses intercellular communication probability, which are calculated from projected expression profiles of paired ligands and receptors (referred to as "interaction strengths"), to deduce intricate communication networks among cell types. Normalized data matrices derived from cells from the ADPKD microenvironment, the normal microenvironment cells, or cells from specific cell subtypes were utilized as input. Interaction strengths were computed with parameters type = truncatedMean and trim = 0.001, offering a quantitative measure of cell communication dynamics.

Differential Analysis and Pathway Enrichment Analysis

Differentially expressed genes in MNPs between the ADPKD and normal microenvironment were identified using the Seurat FindMarkers function. Genes detected in at least 25% of cells were considered as input, with an absolute log fold-change threshold of 1 and a Bonferroni-corrected p value of 0.05 applied for significance assessment.

To evaluate the differences in cell proportions between the ADPKD and normal samples, we applied the Wilcoxon rank-sum test. Meanwhile, we utilized the Mann-Whitney test to determine significant variations in the ECM and collagen scores among distinct sample groups derived from the microarray data (GSE7869).

Pathway enrichment analysis was performed with VISION (version 3.0.1) [32]. Leveraging its capabilities, we probed the functional landscape using the Hallmark

curated gene sets and the Gene Ontology (GO) gene set. All the gene sets were attained through Molecular Signatures Database (version 2023.1, https://www.gsea-msigdb.org/gsea/msigdb).

Gene Regulatory Network Analysis

To infer the intricate gene regulatory relationships, we utilized pySCENIC (version 0.12.1) [33], a Python-based tool to obtain the average regulatory activity of specific transcription factors in T cells. The single-cell expression matrix of T cells from the ADPKD microenvironment was converted to a loom file through the Scanpy package [34]. The analysis was conducted following the guidelines provided on the pySCENIC official website, with the reference genome set as the hg19-tss-10 kb genome file (available at https://resources.aertslab.org/cistarget/databases/homo_sapiens/hg19/refseq_r45/mc9nr/gene_based/). All parameters used in the function were kept at their default settings.

Pseudotime Trajectory Analysis

We employed Monocle v3 to infer the potential development trajectory inherent to T cells and fibroblasts in the ADPKD environment, respectively. The expression matrices of the corresponding cell populations were extracted and subjected to a second round of normalization, followed by scaling and dimension reduction. Then, leveraging the transformed data, Monocle 3 was used to construct the developmental trajectory tree. The initial cells for the development trajectory were selected based on their proliferation properties revealed in pathway enrichment analysis or G2M scores obtained from the Seurat CellCycleScoring function.

Bulk Analysis and Cell-Type Deconvolution

We initially subjected the bulk gene expression matrix from microarray data (GSE7869) to Robust Multichip Average (RMA) normalization. Then, the probes within the matrix were subsequently converted to gene symbols. The expression level of each gene symbol was represented by the corresponding probe exhibiting the highest mean expression across all samples. We employed ComBat [35] analysis through sva packages (version 3.48.0) to alleviate the impact of potential batch effects originating from diverse patient sources.

To deconvolute the expression matrices of microarray, we leveraged CIBSORTx v1.0 [36] within the IOBR package (version 0.99.9). First, a signature matrix representing all major cell lineages from the scRNA-seq data was generated based on the top 2,000 highly variable genes (HVGs) obtained by Seurat. Using this signature matrix, we deconvolute the microarray gene profiles to estimate the relative abundance of the major cell lineages within the microarray datasets.

Results

Single-Cell Transcriptomic Profiling Unveils an Elevated Abundance of Immune Cells and Fibroblasts in ADPKD

We characterized the landscape of kidney cells within a cohort consisting of seven samples and three adjacent normal tissues (Fig. 1a). A total of 111,601 cells were obtained, with 86,197 from the ADPKD microenvironment and 25,404 from the normal microenvironment. Following quality control (online suppl. Fig. S2B), our final dataset was refined to include 93,483 cells. Among these, 74,380 cells originated from the ADPKD and 19,103 cells from the normal microenvironment. After batch correction (Fig. 1b; online suppl. Fig. S2C, D), we performed unsupervised clustering analyses, and the remaining cells were categorized into nine major cell lineages based on established marker genes, including proximal tubule (PT) cells (SLC13A3, DCXR, GPX3), T cells (CD3D, CD3E, TRAC), MNPs (LYZ, CD14, CD68), fibroblasts (FIBs) (PDGFRB, ACTA2, DCN, COL1A1, THY1), B cells (CD79A, MS4A1, CD19), mast cells (KIT, ENPP3), cyst-lining epithelial cells (CDH1, EPCAM, KRT23, KRT18), endothelial cells (PECAM1, VWF), and distal tubule cells (UMOD, DEFB1) (Fig. 1b, c).

The composition of major cell lineages exhibited considerable heterogeneity between the ADPKD and the normal microenvironment, consistent with the findings via snRNA-seq and snATAC-seq [16] (Fig. 1d). Compared to the normal, the ADPKD microenvironment was notably characterized by a higher presence of immune cells, especially T cells (averaging 29.92% in ADPKD vs. 4.11% in normal; Wilcoxon test p value = 0.017) and MNPs (averaging 20.32% in ADPKD vs. 3.10% in normal; Wilcoxon test p value = 0.017), along with an increased abundance of fibroblasts (averaging 17.92% in ADPKD vs. 0.08% in normal; Wilcoxon test p value = 0.017). In total, our analysis identified 15,695 MNPs, with 15,059 (95.9%) originating from the ADPKD microenvironment and a small number from the normal microenvironment. MNPs encompassed a heterogeneous group of immune cells originating from bone marrow progenitors, which included macrophages, monocytes, and dendritic cells [37]. Simultaneously, we discerned 22,639 T cells, primarily from the ADPKD context (21,909; 96.8%) and a

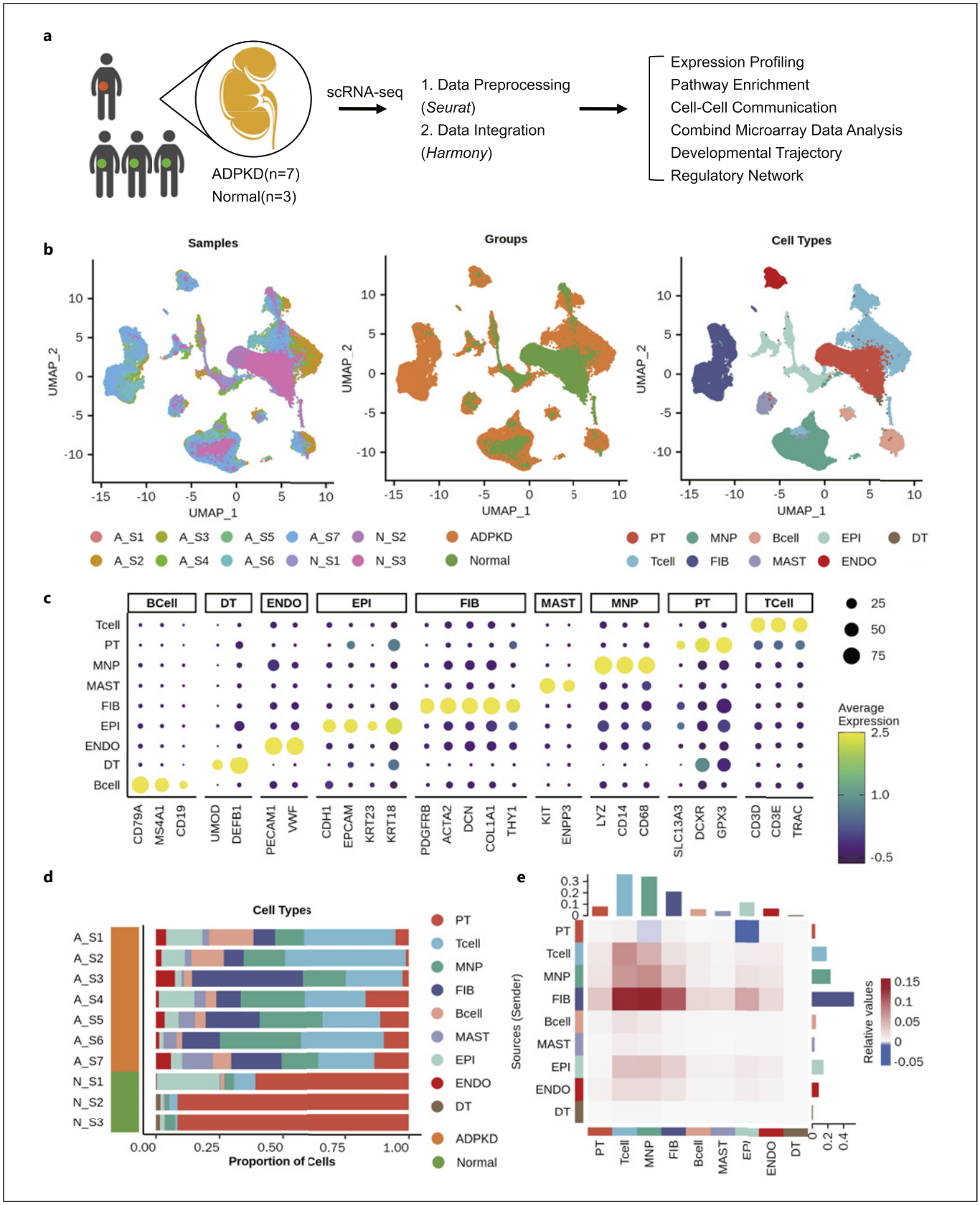

(For legend see next page.)

minor fraction (730; 3.2%) from normal samples. Additionally, 12,774 fibroblasts were detected, with the majority (12,760; 99.9%) originating from the ADPKD microenvironment, and only 14 (0.1%) from normal tissues. The massive increase in immune cells and fibroblasts in patients corresponded with the key pathological feature of PKD – the development of interstitial inflammation and fibrosis [38]. In contrast, the normal kidney microenvironment was predominantly characterized by the presence of PT cells (averaging 8.64% in ADPKD vs. 81.36% in normal; Wilcoxon test p value = 0.017).

In addition to variations in cell proportions, the pattern of cellular interactions is also a significant aspect of characterizing the ADPKD microenvironment. Therefore, we employed CellChat to construct a cell-cell communication network, based on established ligand-receptor pairs, to explore the molecular interactions among cell lineages from both ADPKD and normal. Notably, we observed a significant rise in interactions among MNPs, T cells, and fibroblasts in the ADPKD microenvironment (Fig. 1e), reinforcing the predominant role of these cell lineages and their interactions in the disease development. Conversely, interactions between PT cells and epithelial cells were decreased in the ADPKD microenvironment, likely due to a notable reduction in PT cell counts.

To investigate functional alterations in the ADPKD microenvironment, we conducted pathway enrichment analyses using hallmark gene sets (online suppl. Fig. S3). This revealed strong activation of various inflammation-associated pathways in ADPKD MNPs, including complement pathway, inflammatory responses pathway, IL-6/JAK/STAT3 signaling pathway, and TNFA signaling via NFκB pathway. Given the previously established link between inflammation and cyst progression in ADPKD [38], these findings suggest a potential role for MNPs in ADPKD progression through diverse inflammatory processes. Furthermore, our analysis highlighted the activation of the epithelial-mesenchymal transition (EMT) pathway within ADPKD fibroblasts. EMT symbolizes potential transdifferentiation from epithelial cells into activated fibroblasts, i.e., myofibroblasts, and exacerbates adjacent interstitial fibrosis found in many chronic kidney diseases [39]. Interestingly, we found the enrichment of the apical surface pathway in epithelial cells in the ADPKD environment, aligning with one of the disease's characteristics, apical mispolarization [40]. Collectively, the scRNA-seq profiling provided insights into the distinctive attributes of the ADPKD microenvironment. Among the nine major cell lineages, MNPs, T cells, and fibroblasts emerged as significant contributors to the heterogeneity in molecular interactions and function profiles, suggesting their combined role in forming a specialized microenvironment to foster disease development. To further explore the relationships within and among these three lineages, we conducted a subsequent round of subclustering for more detailed characterization.

Macrophages Exhibit M2-Polarization and Facilitate Cyst-Lining Epithelial Proliferation in the ADPKD Microenvironment

To characterize the alteration in molecular signatures of MNPs in ADPKD, our study employed subclustering, uncovering eight distinct subpopulations within MNPs. Among these, we identified five macrophage subtypes, one classical monocyte subtype (S100A8+ cMono), and two plasmacytoid dendritic cell subtypes (GZMB+ pDC_C1 and S100B+ pDC_C2) (Fig. 2a; online suppl. Fig. S4A).

Macrophages are acknowledged for their inclination to adopt an "M2-like" phenotype, fostering cyst cell proliferation and cyst growth within kidney injury, thereby playing pivotal roles in ADPKD pathogenesis [41]. To further explore the associations between M1/M2 phenotypes and ADPKD, we conducted a comprehensive M1/M2 classification specifically for the five macrophage subtypes within MNPs. This classification relied on M1 and M2 scores derived from gene

Fig. 1. Single-cell transcriptional atlas of ADPKD and control samples. **a** Overview of the workflow. $n = 7$ human ADPKD kidney samples from 1 patient and $n = 5$ control kidney samples from 3 donors were subjected to scRNA-seq profiling. See more in the Methods section. **b** UMAP plots of 93,483 cells from the ADPKD and the normal microenvironment, color-coded by sample number (left), sample type (middle), and major cell lineage (right). See the relationship between the sample number and the original accession number in online supplementary Table S1. **c** Dot plot showing the expression levels of well-established marker genes across major cell lineage. The dot size represents the percentage of cells expressing the marker genes of interest. The color intensity indicates the mean scaled expression of genes within expressing cells. **d** The composition of major cell lineages originated from 10 samples, color-coded by major cell lineage and sample type. **e** Heatmap showing the difference in molecular interactions between the ADPKD and the normal environment. x-axis and y-axis are color-coded by cell lineages. Color in the heatmap represents the relative increase (red) and decrease (blue) of interactions, while the intensity correlates to the relative increase or decrease in value.

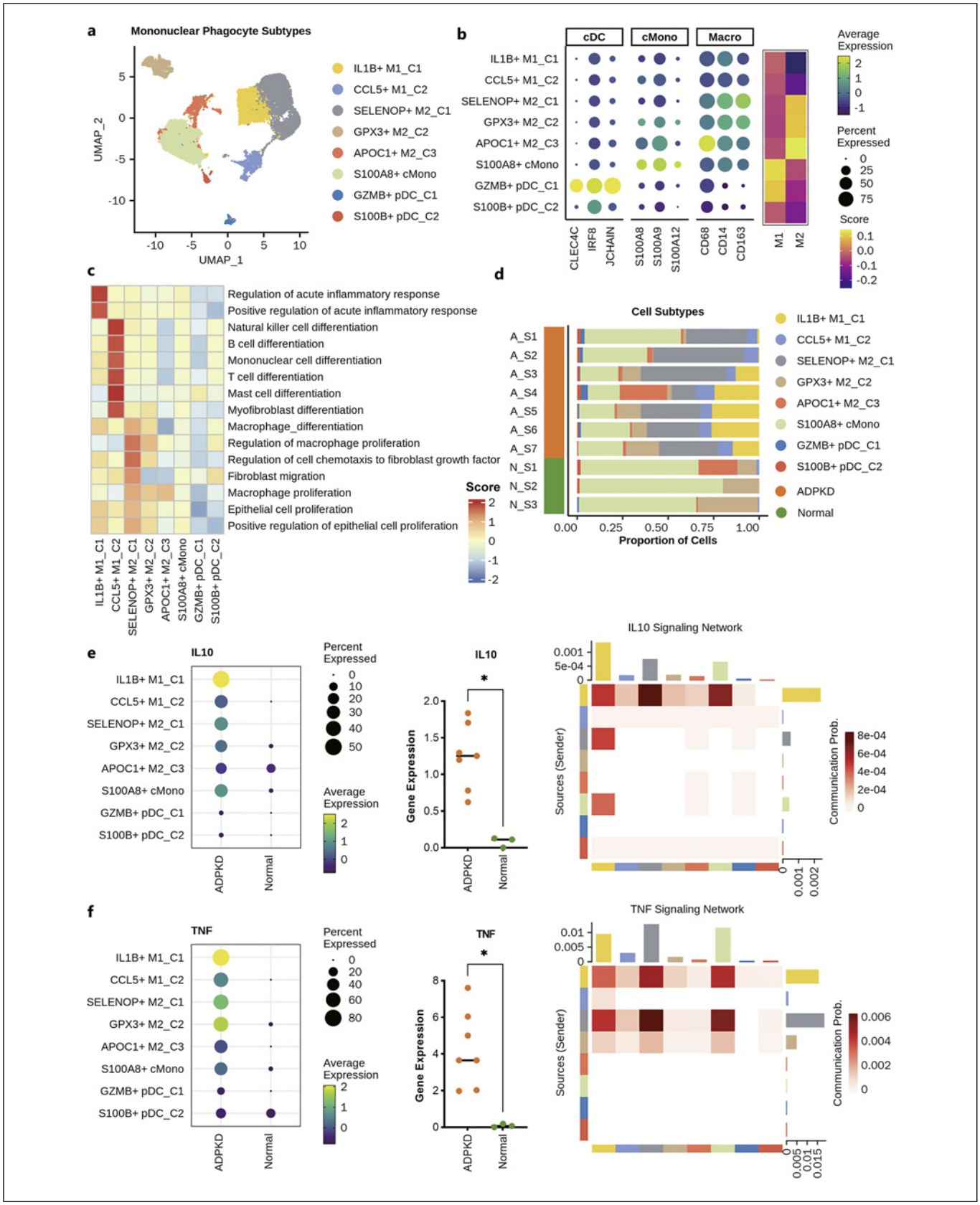

(For legend see next page.)

expression characteristics of M1-like and M2-like macrophages (online suppl. Fig. S4B, C) [28]. Consequently, our analysis identified two distinct M1-like macrophage subtypes (IL1B+ M1_C1 and CCL5+ M1_C2) with higher M1 scores and three subtypes of M2-like macrophages (SELENOP+ M2_C1, GPX3+ M2_C2, and APOC1+ M2_C3), each demonstrating higher M2 scores (Fig. 2b). Among the macrophage subtypes, IL1B+ M1_C1 cells were marked by high expression of inflammatory cytokines, including IL1B, CCL20, CXCL8, and CXCL3, which supported by pathway enrichment analyses that highlighted their association with inflammation-related pathways (Fig. 2c; online suppl. Fig. S5). Likewise, CCL5+ M1_C2 cells predominantly expressed CCL5 and IL32, indicating heterogeneous proinflammatory phenotypes (online suppl. Fig. S4A). Pathway analysis suggests that CCL5+ M1_C2 was associated with the differentiation of multiple immune cells, including NK cells, B cells, mononuclear cells, T cells, mast cells, and myofibroblasts (Fig. 2c). M2-like macrophages demonstrated distinct gene expression profiles relating to M2 polarization, with SELENOP, GPX3, and APOC1 as key markers for each subtype. Among them, SELENOP+M2_C1 was strongly linked to macrophages differentiation and proliferation, epithelial cell proliferation, and fibroblast migration (Fig. 2c). Notably, all M2-like subtypes exhibited high expression of C1QA, recognized as a marker gene for kidney-resident macrophages in cystic disease [42, 43] (online suppl. Fig. S4A), suggesting their potential origin from kidney-resident macrophages, while other subtypes may originate from infiltrating macrophages.

To pinpoint MNP subtypes potentially influencing disease progression, we assessed the proportion of cells within each MNP subset relative to the total MNPs. In the ADPKD microenvironment, a substantial increase in specific macrophage subtypes was evident compared to the normal context. Noteworthy subtypes contributing to this elevation included IL1B+ M1_C1 cells (averaging 15.05% in ADPKD vs. 0.00% in Normal; Wilcoxon test p value = 0.021), CCL5+ M1_C2 cells (averaging 7.20% in ADPKD vs. 0.64% in normal; Wilcoxon test p value = 0.017), and SELENOP+ M2_C1 cells (averaging 33.90% in ADPKD vs. 0.00% in normal; Wilcoxon test p value = 0.021) (Fig. 2d). This elevation pattern was further collaborated by the microarray dataset, which exhibited elevated M1 and M2 scores in the ADPKD cyst samples (online suppl. Fig. S4D).

To further dissect the specific mechanisms governing unique molecular signatures in ADPKD MNPs, we conducted a DEG analysis between ADPKD and normal MNPs. From this, we identified 1,048 DEGs, with 741 upregulated and 307 downregulated (online suppl. Fig. S6A; Table S3). Among these DEGs, IL10, a cytokine known to promote M2-polarization accompanied by increased levels of IL-4 and TGF-β [44], exhibited significant abundance in IL1B+ M1_C1 (Fig. 2e). To infer the target of this signaling cascade, we performed CellChat analysis [31] to quantitatively infer cell-cell communication networks. Our analysis revealed that IL1B+ M1_C1 played a dominant role as the sender, while SELENOP+ M2_C1 served as the receiver in the activated IL-10 signaling network within MNPs (Fig. 2e; online suppl. Fig. S7A). This finding was supported by a prominent upregulation of TGFB1 in ADPKD (online suppl. Fig. S6B), which is primarily produced by T cells and targeted SELENOP+ M2_C1 cells (online suppl. Fig. S7B). Although IL4 was not significantly upregulated (online suppl. Fig. S6B), we found IL4 signaling also targeted SELENOP+ M2_C1 cells, and this signaling was mainly produced by mast cells (online suppl. Fig. S7B). These results suggest that SELENOP+ M2_C1 might undergo M2 polarization under the combined influences of IL1B+ M1_C1, T cells, and mast cells, facilitating cyst cell proliferation and cyst growth [9].

Fig. 2. Comprehensive characterization of MNPs in the ADPKD and the normal microenvironment. **a** UMAP plot of MNPs from the ADPKD and the normal microenvironment, color-coded by cell subtypes. **b** Dot plot (left) and heatmap (right) showing the expression levels of well-established marker genes and the M1/M2 scores across MNP subtypes. Dot size represents the percentage of cells expressing specific marker genes. The color intensity indicates the mean scaled expression of genes within expressing cells and the M1/M2 score. **c** Heatmap showing the enrichment of GO gene sets of the MsigDB in MNP subtypes in the ADPKD environment. Color indicates the logarithm of the mean signature score for cells in their respective group. **d** The composition of MNP subtypes originated from 10 samples, color-coded by MNP subtype and sample type. IL-10 (**e**) and TNF (**f**) signaling characterization. Dot plots (left) showing the expression levels. Dot size represents the percentage of cells expressing IL-10 (**e**) and TNF (**f**). Color intensity indicates the mean scaled expression of IL10 (**e**) and TNF (**f**). Dot plots (middle) showing the mean expressions of IL10 (**e**) and TNF (**f**) in the ADPKD samples and normal samples. p value was calculated by the Wilcoxon test. *, p value <0.05. Heatmaps (right) showing the molecular interactions of IL10 (**e**) and TNF (**f**) signaling among subtypes. x axes and y axes are color-coded by cell lineages. Color intensity represents the relative abundance of interactions.

Another significantly upregulated DEG, TNF, which is linked to cystogenesis through upregulation of FIP-2 (OPTN) and disturbance of PC2 localization [45], was predominantly abundant in IL1B+ M1_C1 cells (Fig. 2f). Cell-cell communication analysis unveiled that TNF signaling was mainly activated within MNPs and T cells. In MNPs, both IL1B+ M1_C1 and SELENOP+ M2_C1 served as both primary sources and target cells (Fig. 2f; online suppl. Fig. S7A). Moreover, the concomitant enrichment of OPTN was observed in CCL5+ M1_C2 cells and GZMB+ pDC_C1 cells (online suppl. Fig. S6C). Although CCL5+ M1_C2 was not the main target of TNF signaling in MNPs, it might still influence the upregulation of OPTN.

Furthermore, cell-cell communication analysis also revealed specific interactions from MNPs to cyst-lining epithelial cells, including HGF and EGF signaling pathways (online suppl. Fig. S7B). The primary source cells for these pathways included IL1B+ M1_C1, SELENOP+ M2_C1, and S100A8+ cMono. The ligand genes, HGF and EGF, were abundant in SELENOP+ M2_C1 and GPX3+ M2_C2, as well as IL1B+ M1_C1, within the ADPKD microenvironment, respectively. Given that both HGF and EGF are well-known stimulators of epithelial cell proliferation [21], our findings suggest that these three specific macrophage subtypes might promote epithelial cell proliferation through these two signaling pathways in the ADPKD microenvironment.

CD4+ T Cells Establish an Immunosuppressive ADPKD Microenvironment in Collaboration with MNPs

Concurrently with the increased presence of MNPs, T cells constituted another substantial component within the expanded immune cell population. To explore the heterogeneity among T cells, subclustering of this major cell lineage identified three distinct CD4+ subtypes (CD4+IL7R+ C1, CD4+TNF+ C2, and CD4+RTKN2+ C3) and four CD8+ subtypes (CD8+NKG7+ C1, CD8+ CCL4L2+ C2, CD8+MGP+ C3, and CD8+STMN1+ C4) (Fig. 3a, b).

CD4+IL7R+ C1 displayed high expression of memory T markers, including IL7R and CCR7, suggesting a memory T-cell phenotype (Fig. 3c). Contrastingly, CD4+TNF+ C2 showcased an enrichment of type 1 helper T cell (Th1) markers, such as IFNG, CXCR3, and TNF (Fig. 3c), indicative of a Th1-like cell population. Both CD4+IL7R+ C1 and CD4+TNF+ C2 were involved in inflammatory processes, with CD4+IL7R+ C1 being active in antigenic stimulus-induced acute inflammatory response (online suppl. Fig. S8A), while CD4+TNF+ C2 strongly associated with inflammatory response and IL6 signaling pathway (online suppl. Fig. S9). Additionally, CD4+RTKN2+ C3 harbored Treg features, expressing high levels of FOXP3 and IL2RA. This finding was corroborated by pySCENIC analysis, which revealed the significant activation of FOXP3, STAT3, and USF1 as transcript regulators [46] (Fig. 3b, c). Besides, CD4+RTKN2+ C3 exhibited the highest exhaustion scores over all subtypes (online suppl. Fig. S8B). Cell counting demonstrated CD4+TNF+ C2 with an average proportion of 16.28% (null of which in normal; Wilcoxon test p value = 0.021) and CD4+RTKN2+ C3 with an average proportion of 2.76% (null of which in normal; Wilcoxon test p value = 0.021) was exclusively identified in the ADPKD microenvironment (Fig. 3d).

All CD8+ subtypes were characterized as effector memory CD8+ T cells, featuring a high expression of GZMA but differing in their specific marker genes NKG7, GZMK, M1TG, and STMN1, respectively (online suppl. Fig. S8B). Notably, CD8+NKG7+ C1 stood out as the highest cytotoxicity scores, featuring an increased expression of cytotoxic genes such as NKG7 and GNLY (online suppl. Fig. S8B). This subtype showed significant enrichment in cytotoxicity-related pathways, such as leukocyte-mediated cytotoxicity regulation and T cell-mediated cytotoxicity (online suppl. Fig. S8A). The CD8+M1TG+ C3 subtype was characterized by high expression of the metallothionein (MTs) family, including MT1G, MT1E, MT1F, MT2A, and MT1X, known for impeding CD8+ T-cell responses and proliferation [47]. Cell counting demonstrated that the overall numbers of CD8+ T cells were equivalent between APPKD and normal microenvironment, suggesting that the distribution of CD8+ T-cell subtypes remains relatively stable in the context of ADPKD (Fig. 3d).

While CD8+ T cells are recognized for their anti-cystogenesis roles and are associated with ADPKD severity [11], the function roles of CD4+ T cells in this context remain under explored. Employing CellChat analysis, we delved deeper into the interactions between T cells and other cells in the ADPKD microenvironment. We observed that CD4+ T cells served as primary receivers in multiple immunosuppressive pathways, including PDL1 [48], CD80, CD86, and ICOS pathways (Fig. 3e; online suppl. Fig. S10–S13), while the main senders are IL1B+ M1_C1, SELENOP+M2_C1, and cMono. In PDL1 signaling, CD4+IL7R+ C1 and CD4+TNF+ C2 were identified as key target cells with a high expression of PDL1 receptor, PD-1 (PDCD1) (Fig. 3e). Notably, PD-1, traditionally associated with

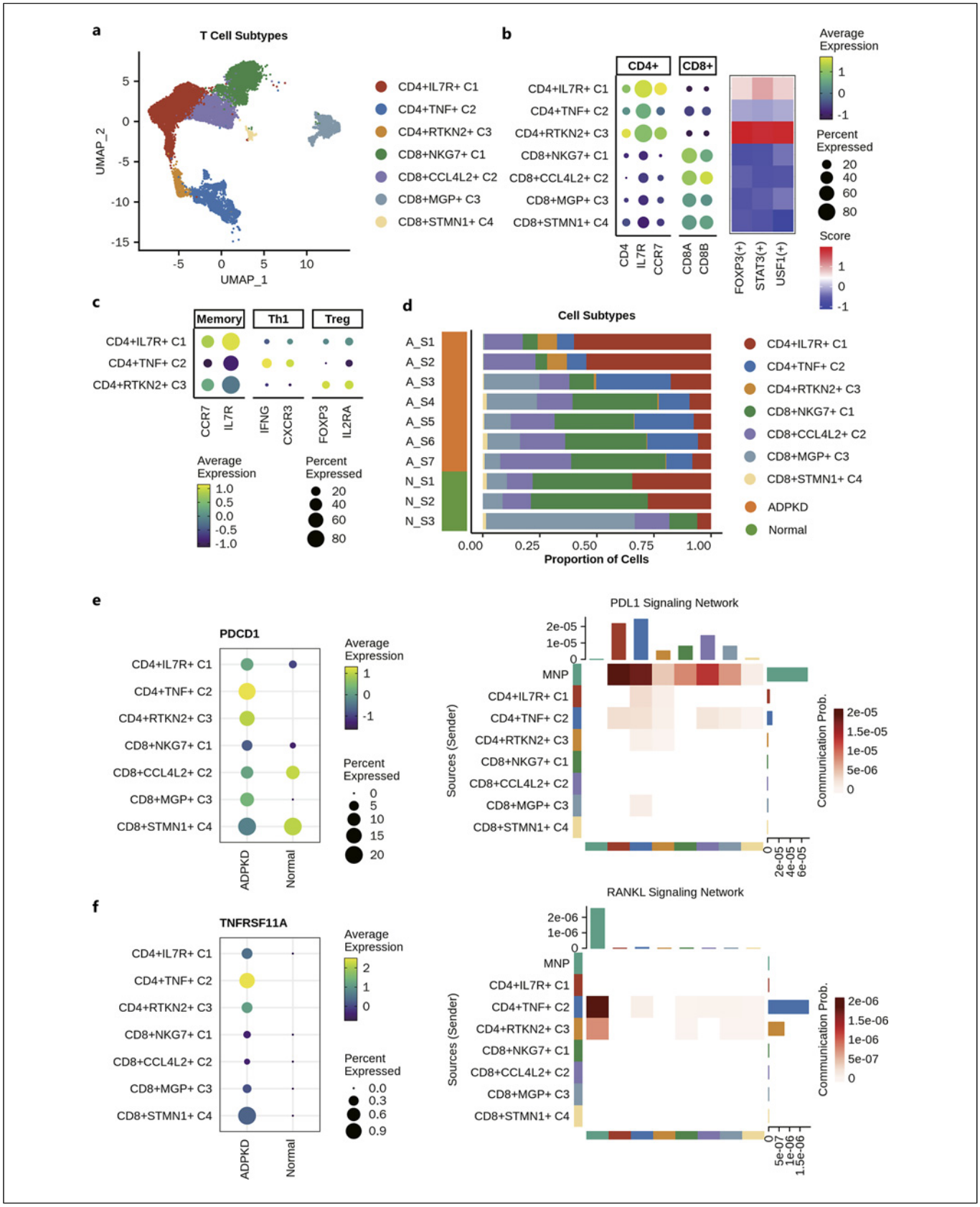

3

(For legend see next page.)

CD8+ T cells in most tumor cells [48], was different from our study. To predict the potential developmental relationship between these two subtypes, we performed pseudo-time trajectory analysis (online suppl. Fig. S8C), further demonstrating differentiation paths originating from CD4+TNF+ C2 cells with branching toward CD4+RTKN2+ C3 cells. This was supported by previous studies that PDL1 signaling could convert Th1 cells to Treg cells [49]. Besides, in other immune checkpoint signaling pathways, CD80 and CD86 signaling, CD4+IL7R+ C1 emerged as the main receivers (online suppl. Figs. S11, S12). Although CD4+RTKN2+ C3 was not the main target, it expressed high levels of the receptor for these pathways including CTLA-4 and ICOS (online suppl. Fig. S8D), indicating properties associated with Treg cells. While CTLA-4 is enriched in Treg cells and ICOS+ Treg cells play a dominant role in the process of immune escape in malignant tumors, CTLA-4 and ICOS synergistically exert an inhibitory function of Tregs [48, 50].

Furthermore, our analysis unveiled the activation of RANKL signaling in T cells. Unlike the immune checkpoint signaling pathways, the pathway exhibited reciprocal dynamics, with CD4+TNF+ C2, predominantly as source cells and GPX3+M2_C2 as target cells in MNPs (Fig. 3f; online suppl. Fig. S12). RANKL signaling pathway functions in inducing TNF transcription in renal epithelial cells [51], suggesting that the activation of TNF signaling within macrophages might partly be attributed to CD4+TNF+ C2.

Fibroblasts Mediated by Multi-Type Cells Show High Functional Heterogeneity in the ADPKD Microenvironment

Utilizing single-cell RNA data, we dissected fibroblasts into eight subtypes, comprising seven subtypes (SYT1+ FIB1, IGF1+ FIB2, CCL4+ FIB3, GRM8+ FIB4, SERPINE2+ FIB5, CFD+ FIB6, and MME+ FIB7) and one myofibroblast (ACTA2+ Myo) (Fig. 4a, c; online suppl. Fig. S14A).

Expanding renal cysts in ADPKD are often surrounded by varying degrees of interstitial fibrosis with ECM accumulation. We observed that nearly all the fibroblasts were derived from the ADPKD microenvironment, with MME+ FIB7 cells being scarcely present in the normal kidney microenvironment (Fig. 4d). Validation through microarray dataset using CIBERSORTx confirmed a heightened fraction of fibroblasts during ADPKD progression, consistent with previous studies indicating that fibroblasts and ECM constitute only a minor proportion of normal kidney tissue volume [52] (Fig. 4b).

Subsequently, to pinpoint cell types contributing to ECM production in ADPKD, we applied ECM and collagen expression scores defined by Kuppe et al. [30], which estimate the expression of collagens, glycoproteins, and proteoglycans. Correspondingly, higher ECM and collagen scores were observed in cyst samples in the bulk data, indicating ECM accumulation in ADPKD (online suppl. Fig. S14B). When comparing ECM scores across all cell lineages, fibroblasts demonstrated the highest ECM scores, followed by endothelial cells and epithelial cells. This suggests the potential involvement of endothelial to mesenchymal transition (EndMT) and EMT in the ADPKD microenvironment (online suppl. Fig. S14C). Within fibroblast subtypes, SYT1+ FIB1, IGF1+ FIB2, and SERPINE2+ FIB5 displayed higher ECM scores, indicative of their role as collagen-producing fibroblasts (online suppl. Fig. S14D, E). Moreover, elevated FAP expression, which regulates the balance of matrix deposition and turnover, was identified in SYT1+ FIB1, IGF1+ FIB2, and SERPINE2+ FIB5 [53] (online suppl. Fig. S14A).

Among these collagen-producing subtypes, SYT1+ FIB1 expressed IGFBP6, a binding protein associated with suppressing fibroblast proliferation [54]. In contrast,

Fig. 3. Comprehensive characterization of T cells in the ADPKD and the normal microenvironment. **a** UMAP plot of T cells from the ADPKD and the normal microenvironment, color-coded by cell subtypes. **b** Dot plot (left) and heatmap (right) of well-established marker genes across T-cell subtypes. The color intensity of the dot plot indicates the mean scaled expression of genes within expressing cells. The dot size represents the percentage of cells expressing the marker genes of interest. The color of the heatmap shows the AUC scores of expression regulation by transcription factors estimated by pySCENIC. **c** Dot plot showing the expression levels of well-established marker genes across CD4+ T-cell subtypes. The dot size represents the percentage of cells expressing the marker genes of interest. The color intensity indicates the mean scaled expression of genes within expressing cells. **d** The composition of T-cell subtypes originated from 10 samples, color-coded by T-cell subtype and sample type. PD-1 (PDCD1) (**e**) and TNFRSF11A (**f**) signaling characterization. Dot plot (left) showing the expression levels. The dot size represents the percentage of cells expressing PD-1 (PDCD1) (**e**) and TNFRSF11A (**f**). The color intensities indicate the mean scaled expression of PD-1 (PDCD1) (**e**) and TNFRSF11A (**f**). Heatmaps (right) showing the molecular interaction of PD-L1 (**e**) and RANKL (**f**) signaling among subtypes. *x* axes and *y* axes are color-coded by cell lineages. Color intensity represents the relative abundance of interactions.

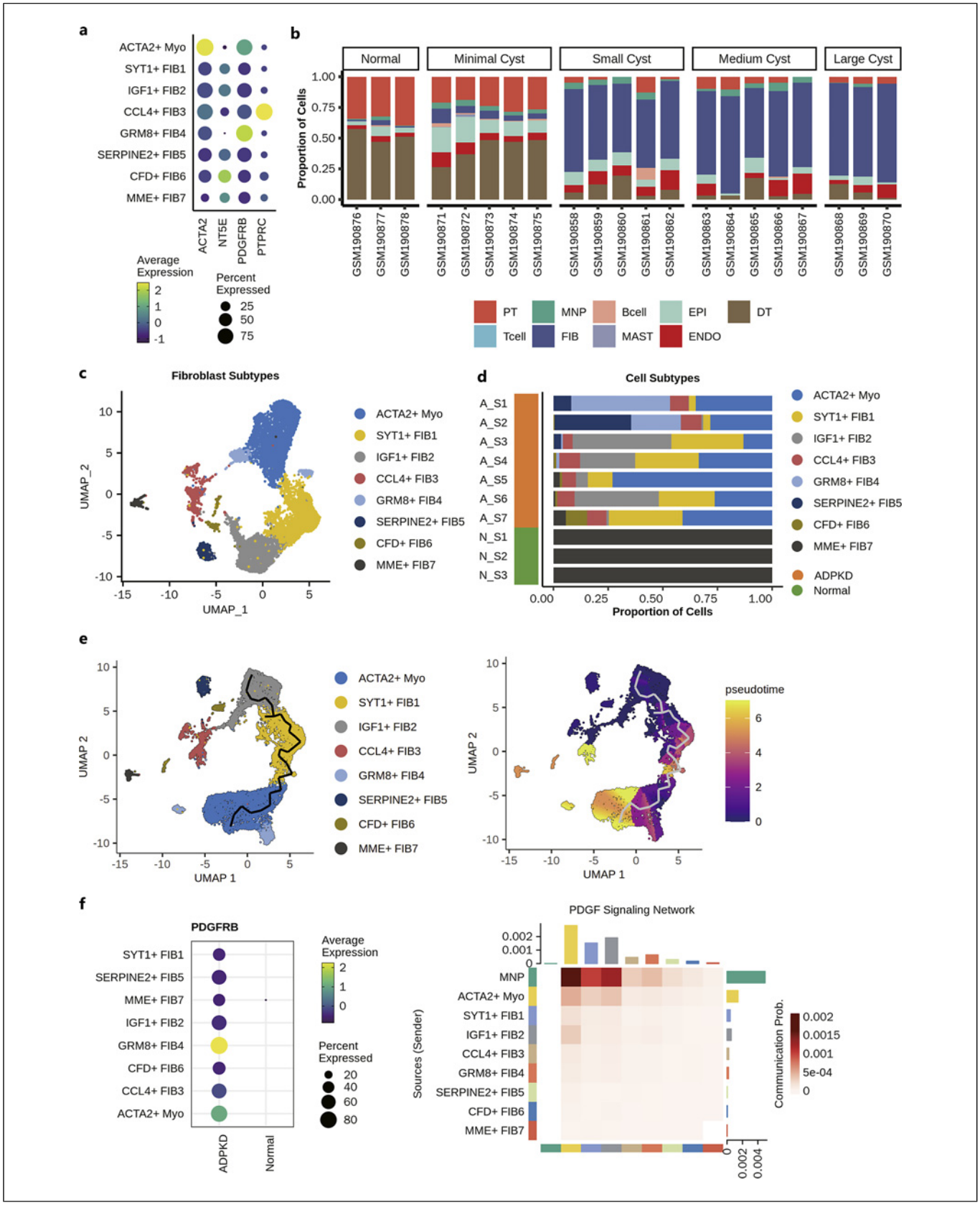

4

(For legend see next page.)

IGF-1+ FIB2 was marked by high expression of IGF-1, which stimulates fibrogenesis potentially via Snail1 upregulation in diabetic murine models [55]. These two subtypes displayed negative and positive associations with fibroblast proliferation, respectively (online suppl. Fig. S14F). SERPINE2+ FIB5 demonstrated enhanced SERPINE2 expression, linked to collagen accumulation and cardiac fibrosis [56]. Pathway enrichment analysis also revealed that both IGF1+ FIB2 and SERPINE2+ FIB5 were strongly associated with collagen-related pathways (online suppl. Fig. S14F).

While the remaining subtypes exhibited less collagen-producing ability, they contribute to other functions in ADPKD progression. CCL4+ FIB3 showed expression of pan-leukocyte marker CD45 (PTPRC) and lacked the resident fibroblast markers CD73 (NT5E) or PDGFBR [57] (Fig. 4b). This suggests that CCL4+ FIB3 could potentially derive from bone marrow-derived fibrocytes, whereas other subtypes likely have tissue-resident properties. Moreover, CCL4+ FIB3 co-expressed inflammatory cytokines such as CCL3, CCL4, CCL5, and IL7R (online suppl. Fig. S14A), probably due to the proinflammatory nature of fibrocytes adopted under injury conditions [58]. Pathway enrichment analysis also revealed that it related to inflammatory processes, including IL-2 signaling and IL-6 signaling (online suppl. Fig. S15), as well as myofibroblast differentiation (online suppl. Fig. S14F). GRM8+ FIB4 was characterized by ANO1 upregulation, a known promoter of cyst growth [59] (online suppl. Fig. S14A). Additionally, CFD+ FIB6, expressing higher levels of PRG4, could regulate fibroblast to myofibroblast differentiation in synovium [60], while MME+ FIB7 has increased expression of PTPRO, potentially facilitating fibrogenesis in liver fibrosis [61] (online suppl. Fig. S14A). Pathway enrichment analysis also revealed that CFD+ FIB6 showed a negative correlation with fibroblast migration, and MME+ FIB7 was related to the regulation process of cell chemotaxis to fibroblast growth factor (online suppl. Fig. S14F).

Myofibroblasts, the key ECM producer, are identifiable by α-smooth muscle actin (α-SMA) [62]. Understanding their origin is crucial for developing antifibrotic therapies in renal fibrosis, a field still not fully understood. By leveraging trajectory inference analyses, we recapitulated the myofibroblast differentiation process and observed that SYT1+ FIB1and IGF1+ FIB2 are enriched in the migrating branch (Fig. 4e), suggesting that myofibroblast originates from IGF1+ FIB2, and SYT1+ FIB1 served as an intermediate development stage. Interestingly, ECM-producing fibroblasts, SYT1+ FIB1, IGF1+ FIB2, and SERPINE2+ FIB5, all displayed higher ECM and collagen scores than ACTA2+Myo (online suppl. Fig. S14D, E), suggesting that unlike in general kidney diseases, specific fibroblast subtypes including SYT1+ FIB1, IGF1+ FIB2, and SERPINE2+ FIB5 are responsible for the ECM accumulation rather than ACTA2 + Myo in the ADPKD microenvironment.

To dissect the complex signaling mechanisms between fibroblast and other cell types, we also conducted cell-cell communication analysis, focusing on pathways related to fibroblast activation and differentiation, including PDGF, Notch, Wnt, and hedgehog signaling. The receptors of these pathways in various fibroblast subtypes showed evident interactions with ligands secreted by other cells. In PDGF signaling pathway, ligands predominantly secreted by IL1B+ M1_C1 and SELENOP+ M2_C1 were received by multiple subtypes including SYT1+ FIB1, IGF1+ FIB2, and ACTA2+ Myo (Fig. 4f; online suppl. Fig. S16A). Interestingly, macrophages promote myofibroblast differentiation and activation through PDGF signaling [63]. However, GRM8+ FIB4 exhibited the highest expression of the PDGF receptor gene, PDGFRB (Fig. 4f). In Notch and Wnt signaling, the main receiver subtype was ACTA2+ Myo, while ACTA2+ Myo itself and SELENOP+ M2_C1 served as sender (online suppl. Fig. S16B, S17). Notch3 takes part in myofibroblast activation as Notch3-knockout mice showed a significant reduction in α-SMA-positive cells [64]. These findings suggested that although ACTA2+ Myo may not be the leading ECM

Fig. 4. Comprehensive characterization of fibroblasts in the ADPKD and the normal microenvironment. **a** The abundances of major cell lineages in the GSE7869 microarray dataset derived from the CIBERSORTx analysis, color-coded by major cell lineages. **b** Dot plot of well-established marker genes across fibroblast cell subtypes. The color intensity of the dot plot indicates the mean scaled expression of genes within expressing cells. The dot size represents the percentage of cells expressing the marker genes of interest. **c** UMAP plot of fibroblasts from the ADPKD and normal microenvironment, color-coded by cell subtypes. **d** The composition of fibroblast subtypes originated from 10 samples, color-coded by fibroblast subtype and sample type. **e** Pseudotime trajectory analysis of fibroblast subtypes. The black curve represents pseudotime trajectory. The UMAP plots are color-coded by different subtypes (left) or pseudotime (right). **f** PDGF signaling characterization. Dot plot (left) showing the expression levels. The dot size represents the percentage of cells expressing PDGF. The color intensity indicates the mean scaled expression of PDGF. Heatmap (right) showing the molecular interaction of PDGF signaling among subtypes. The *x* axis and *y* axis are color-coded by cell lineages. Color intensity represents the relative abundance of interactions.

producer, it still plays a crucial role in myofibroblast activation and differentiation. Additionally, hedgehog signaling was activated in epithelial cells and fibroblasts, particularly in SYT1+ FIB1 and IGF1+ FIB2 (online suppl. Fig. S16B).

Discussion

In this study, we conducted a comprehensive scRNA-seq analysis of both ADPKD and normal kidney tissue, aiming to characterize key cellular lineages and their interactions in the ADPKD microenvironment. This investigation uncovered a spectrum of heterogeneous cell subtypes and elucidated their intricate interactions, providing insights into the dynamics of ADPKD progression. Recent studies based on single-cell transcriptome have detailed the cellular composition of the normal kidney, predominated by PT cells and sparse immune cell presence [19, 65]. In contrast, our analysis revealed a massive increase of immune and stromal cells in ADPKD, especially MNPs, T cells, and fibroblasts. Prior work dissected organ-specific and stromal cell subpopulations, including proximal tubular cells, collecting duct cells, and fibroblasts [16]. Our findings here fully corroborate scRNA-seq data and extend it across immune cells, offering a more comprehensive understanding of the cellular landscapes in ADPKD kidneys.

The proliferation of cyst-lining epithelial cells is the crucial characteristic of ADPKD microenvironments, predominantly driven by soluble factors from M2-like macrophages [9, 66]. Furthermore, recent reports indicate that M2 polarization-induced polyamine production can reduce primary cilia length by disrupting the PC1/PC2 complex [67]. Our study identified a specific macrophage subtype, SELENOP+ M2_C1, which underwent transdifferentiation into an "M2-like" phenotype under the combined influence of IL-10 from IL1B+ M1_C1 cells, IL-4 from T cells, and TGF-β from mast cells. SELENOP+ M2_C1 macrophages were observed to be the source cells of TNF, HGF, EGF, and Wnt signaling pathways. In vitro, Pkd1−/− cells demonstrated a c-Met-dependent upregulation of the PI3K/Akt/mTOR signaling, potentially accelerating cyst development [68, 69]. Given HGFs established function in kidney tubule growth, mediated by paracrine interactions with endothelial cells and macrophages [70], we hypothesize that SELENOP+ M2_C1 is the principal immune cell type driving cyst proliferation and represents a promising therapeutic target for ADPKD. Furthermore, SELENOP+ M2_C1 and GPX3+ M2_C2 displayed high expression of C1QA and CD206 (MRC1), suggesting characteristics of resident macrophage phenotype [71].

Regarding the immunosuppressive aspect of ADPKD, a suppressive milieu was generally found in the microenvironment, characterized by the activation of the immune checkpoint pathway. Key pathways involved include those mediated by PDL1, CD80, and CD86, which are secreted by IL1B+ M1_C1, SELENOP+M2_C1 as well as cMono cells, and interacted with receptors on CD4+IL7R+ C1 and CD4+TNF+ C2 cells. Notably, CD4+TNF+C2 cells exhibited a high expression of IFNG and are indicative of a Th1 phenotype. This subset of CD4+ T cells is comparable to those infiltrating kidneys in murine models post-ischemia-reperfusion injury, which modulated the injury response through IFN-γ [72]. Our findings suggested that CD4+TNF+ C2 might be activated through immune checkpoint pathways, contributing to an immunosuppressive environment. Although the exact mechanism linking immunosuppression and ADPKD progression remains unclear, it is hypothesized that blocking both PD-1 and CTLA-4 could enhance the quantity and activation of CD8+ T cells, thereby affecting cyst expansion [48].

Interstitial fibrosis, a hallmark of chronic kidney disease, manifests to varying extents regardless of its underlying etiology. Heterogeneous fibroblasts were identified in ADPKD microenvironments as ECM producers. Distinguishing from conventional tumor development or wound healing processes, we surprisingly observed that SYT1+ FIB1, IGF1+ FIB2, and SERPINE2+ FIB5 were the primary contributors to ECM accumulation, rather than ACTA2+ myofibroblasts. The activation and proliferation of these ECM-producing cells are mediated by multiple signaling pathways. These included PDGF signaling pathway, activated by IL1B+ M1_C1 and SELENOP+ M2_C1, Wnt signaling driven by SELENOP+ M2_C1, and hedgehog signaling pathway initiated by cyst-lining epithelial cells. These insights highlighted the complex role of macrophages in fibrosis development in the ADPKD microenvironment. Although ACTA2+ myofibroblasts are not the primary ECM producer, previous studies have revealed that depleting α-SMA expressing myofibroblasts could significantly reduce cyst growth and epithelial cell proliferation [73].

However, we acknowledged certain limitations in this study. The sample size was relatively small and a larger cohort with diverse patient populations in ADPKD would provide more robust and generalizable insights. Additionally, while our study highlighted potential signaling pathways and interactions, further experimental

validation is imperative to establish their functional significance. To improve the accuracy of microenvironment localization, future studies could incorporate spatial transcriptomics analysis, which would enable a more precise mapping of the ADPKD microenvironment and help uncover more specific cellular interactions that drive disease progression.

In summary, our study leveraged single-cell sequencing data to unveil the intricate landscape of immune cells and fibroblasts within the ADPKD microenvironment. We observed the general increase abundances in MNPs, T cells, and fibroblasts in the ADPKD microenvironment, forming a complex interaction network that affects ADPKD progression. SELENOP+ M2_C1, influenced by IL1B+ M1_C1, T cells, and mast cells, underwent a phenotypic shift to an "M2-like" state, promoting cyst-lining epithelial proliferation through HGF and EGF signaling pathways. CD4+ T cells were activated through PDL1 signaling by IL1B+ M1_C1 and SELENOP+ M2_C1, creating an immunosuppressive milieu. Moreover, SYT1+ FIB1, IGF1+ FIB2, and SERPINE2+ FIB5 emerged as the primary contributors to fibrosis, with their activation and proliferation influenced by macrophages, T cells, and fibroblasts themselves. These novel insights may offer profound perspectives into future endeavors to improve ADPKD diagnostics and therapeutics.

Statement of Ethics

An ethics statement was not required for this study type since no human or animal subjects or materials were used.

Conflict of Interest Statement

The authors have no conflicts of interest to declare.

Funding Sources

This work was supported by the National Natural Science Foundation of China (grant No. 82000536 to N.J.) and the National Key R&D Program of China (grant No. 2022YFC2705103, 2022YFC2705101 to J.M.). The funders had no role in study design, data collection, and analysis, decision to publish, or preparation of the manuscript. We thank Wondersgene Biotech Co., Ltd. (Tianjin, China) for the bioinformatics analysis support.

Author Contributions

Conceived and designed research: F.L., N.J., and J.M.; analyzed data: F.L., X.L., Q.L., J.G., Q.S., and J.S.; prepared figures: X.L., Q.L., J.G., Q.S., and J.S.; drafted manuscript: F.L. and X.L.; edited and revised manuscript: N.J., and J.M., and approved final version of manuscript: N.J. and J.M.

Data Availability Statement

The single-cell transcriptome data underlying this article are publicly available in NCBI Sequence Read Archive (SRA) using the BioProject accession numbers PRJNA679848 [17] and PRJNA544431 [19]. The transcriptomic data from bulk tissues originated from the Gene Expression Omnibus database (GEO), accessed under the identifier GSE7869 [20]. For reproducibility, all programming codes and scripts are provided in our GitHub repository: https://github.com/FragmentsLi/ADPKD.

References

1 Cornec-Le Gall E, Alam A, Perrone RD. Autosomal dominant polycystic kidney disease. Lancet. 2019;393(10174):919–35. https://doi.org/10.1016/S0140-6736(18)32782-X

2 Chebib FT, Torres VE. Autosomal dominant polycystic kidney disease: core curriculum 2016. Am J Kidney Dis. 2016;67(5):792–810. https://doi.org/10.1053/j.ajkd.2015.07.037

3 Praetorius HA, Spring KR. A physiological view of the primary cilium. Annu Rev Physiol. 2005;67:515–29. https://doi.org/10.1146/annurev.physiol.67.040403.101353

4 Torres VE, Harris PC, Pirson Y. Autosomal dominant polycystic kidney disease. Lancet. 2007;369(9569):1287–301. https://doi.org/10.1016/S0140-6736(07)60601-1

5 Anders HJ, Ryu M. Renal microenvironments and macrophage phenotypes determine progression or resolution of renal inflammation and fibrosis. Kidney Int. 2011;80(9):915–25. https://doi.org/10.1038/ki.2011.217

6 Matsumoto K, Xavier S, Chen J, Kida Y, Lipphardt M, Ikeda R, et al. Instructive role of the microenvironment in preventing renal fibrosis. Stem Cells Transl Med. 2017;6(3):992–1005. https://doi.org/10.5966/sctm.2016-0095

7 Seeger-Nukpezah T, Geynisman DM, Nikonova AS, Benzing T, Golemis EA. The hallmarks of cancer: relevance to the pathogenesis of polycystic kidney disease. Nat Rev Nephrol. 2015;11(9):515–34. https://doi.org/10.1038/nrneph.2015.46

8 Heidegger I, Pircher A, Pichler R. Targeting the tumor microenvironment in renal cell cancer biology and therapy. Front Oncol. 2019;9:490. https://doi.org/10.3389/fonc.2019.00490

9 Swenson-Fields KI, Vivian CJ, Salah SM, Peda JD, Davis BM, van Rooijen N, et al. Macrophages promote polycystic kidney disease progression. Kidney Int. 2013;83(5):855–64. https://doi.org/10.1038/ki.2012.446

10 Yang Y, Chen M, Zhou J, Lv J, Song S, Fu L, et al. Interactions between macrophages and cyst-lining epithelial cells promote kidney cyst growth in pkd1-deficient mice. J Am Soc Nephrol. 2018;29(9):2310–25. https://doi.org/10.1681/ASN.2018010074

11 Kleczko EK, Marsh KH, Tyler LC, Furgeson SB, Bullock BL, Altmann CJ, et al. CD8(+) T cells modulate autosomal dominant polycystic kidney disease progression. Kidney Int. 2018;94(6):1127–40. https://doi.org/10.1016/j.kint.2018.06.025

12 Terabayashi T, Germino GG, Menezes LF. Pathway identification through transcriptome analysis. Cell Signal. 2020;74:109701. https://doi.org/10.1016/j.cellsig.2020.109701
13 Su C, Lv Y, Lu W, Yu Z, Ye Y, Guo B, et al. Single-cell RNA sequencing in multiple pathologic types of renal cell carcinoma revealed novel potential tumor-specific markers. Front Oncol. 2021;11:719564. https://doi.org/10.3389/fonc.2021.719564
14 Zhang Y, Narayanan SP, Mannan R, Raskind G, Wang X, Vats P, et al. Single-cell analyses of renal cell cancers reveal insights into tumor microenvironment, cell of origin, and therapy response. Proc Natl Acad Sci U S A. 2021;118(24):e2103240118. https://doi.org/10.1073/pnas.2103240118
15 Shi Y, Zhang Q, Bi H, Lu M, Tan Y, Zou D, et al. Decoding the multicellular ecosystem of vena caval tumor thrombus in clear cell renal cell carcinoma by single-cell RNA sequencing. Genome Biol. 2022;23(1):87. https://doi.org/10.1186/s13059-022-02651-9
16 Muto Y, Dixon EE, Yoshimura Y, Wu H, Omachi K, Ledru N, et al. Defining cellular complexity in human autosomal dominant polycystic kidney disease by multimodal single cell analysis. Nat Commun. 2022;13(1):6497. https://doi.org/10.1038/s41467-022-34255-z
17 Li Q, Wang Y, Deng W, Liu Y, Geng J, Yan Z, et al. Heterogeneity of cell composition and origin identified by single-cell transcriptomics in renal cysts of patients with autosomal dominant polycystic kidney disease. Theranostics. 2021;11(20):10064–73. https://doi.org/10.7150/thno.57220
18 Li LX, Zhang X, Zhang H, Agborbesong E, Zhou JX, Calvet JP, et al. Single-cell and CellChat resolution identifies collecting duct cell subsets and their communications with adjacent cells in PKD kidneys. Cells. 2022;12(1):45. https://doi.org/10.3390/cells12010045
19 Liao J, Yu Z, Chen Y, Bao M, Zou C, Zhang H, et al. Single-cell RNA sequencing of human kidney. Sci Data. 2020;7(1):4. https://doi.org/10.1038/s41597-019-0351-8
20 Song X, Di Giovanni V, He N, Wang K, Ingram A, Rosenblum ND, et al. Systems biology of Autosomal Dominant Polycystic Kidney Disease (ADPKD): computational identification of gene expression pathways and integrated regulatory networks. Hum Mol Genet. 2009;18(13):2328–43. https://doi.org/10.1093/hmg/ddp165
21 Hao Y, Hao S, Andersen-Nissen E, Mauck WM 3rd, Zheng S, Butler A, et al. Integrated analysis of multimodal single-cell data. Cell. 2021;184(13):3573–87.e29. https://doi.org/10.1016/j.cell.2021.04.048
22 Korsunsky I, Millard N, Fan J, Slowikowski K, Zhang F, Wei K, et al. Fast, sensitive and accurate integration of single-cell data with Harmony. Nat Methods. 2019;16(12):1289–96. https://doi.org/10.1038/s41592-019-0619-0
23 Dutertre CA, Becht E, Irac SE, Khalilnezhad A, Narang V, Khalilnezhad S, et al. Single-cell analysis of human mononuclear phagocytes reveals subset-defining markers and identifies circulating inflammatory dendritic cells. Immunity. 2019;51(3):573–89.e8. https://doi.org/10.1016/j.immuni.2019.08.008
24 Schupp JC, Khanal S, Gomez JL, Sauler M, Adams TS, Chupp GL, et al. Single-cell transcriptional archetypes of airway inflammation in cystic fibrosis. Am J Respir Crit Care Med. 2020;202(10):1419–29. https://doi.org/10.1164/rccm.202004-0991OC
25 Mulder K, Patel AA, Kong WT, Piot C, Halitzki E, Dunsmore G, et al. Cross-tissue single-cell landscape of human monocytes and macrophages in health and disease. Immunity. 2021;54(8):1883–900.e5. https://doi.org/10.1016/j.immuni.2021.07.007
26 Suryawanshi H, Yang H, Lubetzky M, Morozov P, Lagman M, Thareja G, et al. Detection of infiltrating fibroblasts by single-cell transcriptomics in human kidney allografts. PLoS One. 2022;17(6):e0267704. https://doi.org/10.1371/journal.pone.0267704
27 Hu C, Li T, Xu Y, Zhang X, Li F, Bai J, et al. CellMarker 2.0: an updated database of manually curated cell markers in human/mouse and web tools based on scRNA-seq data. Nucleic Acids Res. 2023;51(D1):D870–6. https://doi.org/10.1093/nar/gkac947
28 Martinez FO, Gordon S, Locati M, Mantovani A. Transcriptional profiling of the human monocyte-to-macrophage differentiation and polarization: new molecules and patterns of gene expression. J Immunol. 2006;177(10):7303–11. https://doi.org/10.4049/jimmunol.177.10.7303
29 Zhang JY, Wang XM, Xing X, Xu Z, Zhang C, Song JW, et al. Single-cell landscape of immunological responses in patients with COVID-19. Nat Immunol. 2020;21(9):1107–18. https://doi.org/10.1038/s41590-020-0762-x
30 Kuppe C, Ibrahim MM, Kranz J, Zhang X, Ziegler S, Perales-Patón J, et al. Decoding myofibroblast origins in human kidney fibrosis. Nature. 2021;589(7841):281–6. https://doi.org/10.1038/s41586-020-2941-1
31 Jin S, Guerrero-Juarez CF, Zhang L, Chang I, Ramos R, Kuan CH, et al. Inference and analysis of cell-cell communication using CellChat. Nat Commun. 2021;12(1):1088. https://doi.org/10.1038/s41467-021-21246-9
32 DeTomaso D, Jones MG, Subramaniam M, Ashuach T, Ye CJ, Yosef N. Functional interpretation of single cell similarity maps. Nat Commun. 2019;10(1):4376. https://doi.org/10.1038/s41467-019-12235-0
33 Van de Sande B, Flerin C, Davie K, De Waegeneer M, Hulselmans G, Aibar S, et al. A scalable SCENIC workflow for single-cell gene regulatory network analysis. Nat Protoc. 2020;15(7):2247–76. https://doi.org/10.1038/s41596-020-0336-2
34 Wolf FA, Angerer P, Theis FJ. SCANPY: large-scale single-cell gene expression data analysis. Genome Biol. 2018;19(1):15. https://doi.org/10.1186/s13059-017-1382-0
35 Johnson WE, Li C, Rabinovic A. Adjusting batch effects in microarray expression data using empirical Bayes methods. Biostatistics. 2007;8(1):118–27. https://doi.org/10.1093/biostatistics/kxj037
36 Newman AM, Steen CB, Liu CL, Gentles AJ, Chaudhuri AA, Scherer F, et al. Determining cell type abundance and expression from bulk tissues with digital cytometry. Nat Biotechnol. 2019;37(7):773–82. https://doi.org/10.1038/s41587-019-0114-2
37 Chow A, Brown BD, Merad M. Studying the mononuclear phagocyte system in the molecular age. Nat Rev Immunol. 2011;11(11):788–98. https://doi.org/10.1038/nri3087
38 Song CJ, Zimmerman KA, Henke SJ, Yoder BK. Inflammation and fibrosis in polycystic kidney disease. Results Probl Cell Differ. 2017;60:323–44. https://doi.org/10.1007/978-3-319-51436-9_12
39 Fragiadaki M, Macleod FM, Ong ACM. The controversial role of fibrosis in autosomal dominant polycystic kidney disease. Int J Mol Sci. 2020;21(23):8936. https://doi.org/10.3390/ijms21238936
40 Wilson PD, Devuyst O, Li X, Gatti L, Falkenstein D, Robinson S, et al. Apical plasma membrane mispolarization of NaK-ATPase in polycystic kidney disease epithelia is associated with aberrant expression of the beta2 isoform. Am J Pathol. 2000;156(1):253–68. https://doi.org/10.1016/s0002-9440(10)64726-8
41 Karihaloo A, Koraishy F, Huen SC, Lee Y, Merrick D, Caplan MJ, et al. Macrophages promote cyst growth in polycystic kidney disease. J Am Soc Nephrol. 2011;22(10):1809–14. https://doi.org/10.1681/ASN.2011010084
42 Zimmerman KA, Bentley MR, Lever JM, Li Z, Crossman DK, Song CJ, et al. Single-cell RNA sequencing identifies candidate renal resident macrophage gene expression signatures across species. J Am Soc Nephrol. 2019;30(5):767–81. https://doi.org/10.1681/ASN.2018090931
43 Li Z, Zimmerman KA, Yoder BK. Resident macrophages in cystic kidney disease. Kidney360. 2021;2(1):167–75. https://doi.org/10.34067/KID.0006052020
44 Wei W, Zhao Y, Zhang Y, Jin H, Shou S. The role of IL-10 in kidney disease. Int Immunopharmacol. 2022;108:108917. https://doi.org/10.1016/j.intimp.2022.108917
45 Li X, Magenheimer BS, Xia S, Johnson T, Wallace DP, Calvet JP, et al. A tumor necrosis factor-alpha-mediated pathway promoting autosomal dominant polycystic kidney disease. Nat Med. 2008;14(8):863–8. https://doi.org/10.1038/nm1783
46 Liu Y, Shi JZ, Jiang R, Liu SF, He YY, van der Vorst EPC, et al. Regulatory T cell-related gene indicators in pulmonary hypertension. Front Pharmacol. 2022;13:908783. https://doi.org/10.3389/fphar.2022.908783
47 Youn J, Lynes MA. Metallothionein-induced suppression of cytotoxic T lymphocyte function: an important immunoregulatory control. Toxicol Sci. 1999;52(2):199–208. https://doi.org/10.1093/toxsci/52.2.199

48 Kleczko EK, Nguyen DT, Marsh KH, Bauer CD, Li AS, Monaghan MLT, et al. Immune checkpoint activity regulates polycystic kidney disease progression. JCI Insight. 2023;8(12):e161318. https://doi.org/10.1172/jci.insight.161318
49 Amarnath S, Mangus CW, Wang JC, Wei F, He A, Kapoor V, et al. The PDL1-PD1 axis converts human TH1 cells into regulatory T cells. Sci Transl Med. 2011;3(111):111ra120. https://doi.org/10.1126/scitranslmed.3003130
50 Li DY, Xiong XZ. ICOS(+) Tregs: a functional subset of Tregs in immune diseases. Front Immunol. 2020;11:2104. https://doi.org/10.3389/fimmu.2020.02104
51 Zhou JX, Fan LX, Li X, Calvet JP, Li X. TNFα signaling regulates cystic epithelial cell proliferation through Akt/mTOR and ERK/MAPK/Cdk2 mediated Id2 signaling. PLoS One. 2015;10(6):e0131043. https://doi.org/10.1371/journal.pone.0131043
52 Norman J. Fibrosis and progression of Autosomal Dominant Polycystic Kidney Disease (ADPKD). Biochim Biophys Acta. 2011;1812(10):1327–36. https://doi.org/10.1016/j.bbadis.2011.06.012
53 Duffield JS. Cellular and molecular mechanisms in kidney fibrosis. J Clin Investig. 2014;124(6):2299–306. https://doi.org/10.1172/JCI72267
54 Raykha C, Crawford J, Gan BS, Fu P, Bach LA, O'Gorman DB. IGF-II and IGFBP-6 regulate cellular contractility and proliferation in Dupuytren's disease. Biochim Biophys Acta. 2013;1832(10):1511–9. https://doi.org/10.1016/j.bbadis.2013.04.018
55 Dong R, Yu J, Yu F, Yang S, Qian Q, Zha Y. IGF-1/IGF-1R blockade ameliorates diabetic kidney disease through normalizing Snail1 expression in a mouse model. Am J Physiol Endocrinol Metab. 2019;317(4):E686–98. https://doi.org/10.1152/ajpendo.00071.2019
56 Li X, Zhao D, Guo Z, Li T, Qili M, Xu B, et al. Overexpression of SerpinE2/protease nexin-1 contribute to pathological cardiac fibrosis via increasing collagen deposition. Sci Rep. 2016;6:37635. https://doi.org/10.1038/srep37635
57 Sato Y, Yanagita M. Functional heterogeneity of resident fibroblasts in the kidney. Proc Jpn Acad Ser B Phys Biol Sci. 2019;95(8):468–78. https://doi.org/10.2183/pjab.95.033
58 Reilkoff RA, Bucala R, Herzog EL. Fibrocytes: emerging effector cells in chronic inflammation. Nat Rev Immunol. 2011;11(6):427–35. https://doi.org/10.1038/nri2990
59 Cabrita I, Kraus A, Scholz JK, Skoczynski K, Schreiber R, Kunzelmann K, et al. Cyst growth in ADPKD is prevented by pharmacological and genetic inhibition of TMEM16A in vivo. Nat Commun. 2020;11(1):4320. https://doi.org/10.1038/s41467-020-18104-5
60 Qadri M, Jay GD, Zhang LX, Richendrfer H, Schmidt TA, Elsaid KA. Proteoglycan-4 regulates fibroblast to myofibroblast transition and expression of fibrotic genes in the synovium. Arthritis Res Ther. 2020;22(1):113. https://doi.org/10.1186/s13075-020-02207-x
61 Zhang X, Tan Z, Wang Y, Tang J, Jiang R, Hou J, et al. PTPRO-associated hepatic stellate cell activation plays a critical role in liver fibrosis. Cell Physiol Biochem. 2015;35(3):885–98. https://doi.org/10.1159/000369746
62 Yuan Q, Tan RJ, Liu Y. Myofibroblast in kidney fibrosis: origin, activation, and regulation. Adv Exp Med Biol. 2019;1165:253–83. https://doi.org/10.1007/978-981-13-8871-2_12
63 Buhl EM, Djudjaj S, Babickova J, Klinkhammer BM, Folestad E, Borkham-Kamphorst E, et al. The role of PDGF-D in healthy and fibrotic kidneys. Kidney Int. 2016;89(4):848–61. https://doi.org/10.1016/j.kint.2015.12.037
64 Djudjaj S, Chatziantoniou C, Raffetseder U, Guerrot D, Dussaule JC, Boor P, et al. Notch-3 receptor activation drives inflammation and fibrosis following tubulointerstitial kidney injury. J Pathol. 2012;228(3):286–99. https://doi.org/10.1002/path.4076
65 Hansen J, Sealfon R, Menon R, Eadon MT, Lake BB, Steck B, et al. A reference tissue atlas for the human kidney. Sci Adv. 2022;8(23):eabn4965. https://doi.org/10.1126/sciadv.abn4965
66 Peda JD, Salah SM, Wallace DP, Fields PE, Grantham CJ, Fields TA, et al. Autocrine IL-10 activation of the STAT3 pathway is required for pathological macrophage differentiation in polycystic kidney disease. Dis Model Mech. 2016;9(9):1051–61. https://doi.org/10.1242/dmm.024745
67 Yang Y, Zhou J, Zhang D, Lv J, Chen M, Wang C, et al. Dehydration accelerates cytogenesis and cyst growth in Pkd1(-/-) mice by regulating macrophage M2 polarization. Inflammation. 2023;46(4):1272–89. https://doi.org/10.1007/s10753-023-01806-5
68 Qin S, Taglienti M, Nauli SM, Contrino L, Takakura A, Zhou J, et al. Failure to ubiquitinate c-Met leads to hyperactivation of mTOR signaling in a mouse model of autosomal dominant polycystic kidney disease. J Clin Investig. 2010;120(10):3617–28. https://doi.org/10.1172/JCI41531
69 Ikeda K, Kusaba T, Tomita A, Watanabe-Uehara N, Ida T, Kitani T, et al. Diverse receptor tyrosine kinase phosphorylation in urine-derived tubular epithelial cells from autosomal dominant polycystic kidney disease patients. Nephron. 2020;144(10):525–36. https://doi.org/10.1159/000509419
70 Matsumoto K, Nakamura T. Hepatocyte growth factor: renotropic role and potential therapeutics for renal diseases. Kidney Int. 2001;59(6):2023–38. https://doi.org/10.1046/j.1523-1755.2001.00717.x
71 Li Z, Zimmerman KA, Cherakara S, Chumley PH, Collawn JF, Wang J, et al. A kidney resident macrophage subset is a candidate biomarker for renal cystic disease in preclinical models. Dis Model Mech. 2023;16(1):dmm049810. https://doi.org/10.1242/dmm.049810
72 Burne MJ, Daniels F, El Ghandour A, Mauiyyedi S, Colvin RB, O'Donnell MP, et al. Identification of the CD4(+) T cell as a major pathogenic factor in ischemic acute renal failure. J Clin Investig. 2001;108(9):1283–90. https://doi.org/10.1172/JCI12080
73 Dwivedi N, Jamadar A, Mathew S, Fields TA, Rao R. Myofibroblast depletion reduces kidney cyst growth and fibrosis in autosomal dominant polycystic kidney disease. Kidney Int. 2023;103(1):144–55. https://doi.org/10.1016/j.kint.2022.08.036